



Numerical investigation into the effect of surface wettability in pool boiling heat transfer with a stochastic-automata model



C. Marcel^{a,*}, A. Clause^b, C. Frankiewicz^c, A. Betz^d, D. Attinger^c

^a CNEA-CONICET and Balseiro Institute, Bariloche, Argentina

^b CNEA-CONICET and National University of Central Buenos Aires, Tandil, Argentina

^c Iowa State University, Ames, IN, USA

^d Kansas State University, Manhattan, KS, USA

ARTICLE INFO

Article history:

Received 24 October 2016

Received in revised form 2 April 2017

Accepted 8 April 2017

ABSTRACT

Surface wettability is a key property in boiling heat transfer that influences heat-removal mechanisms and/or change their relative relevance. An automata model for pool boiling heat transfer is provided with rules to simulate heat transfer considering the influence of the contact angle. Free bubbles are modeled as a population of virtual spheres that change their geometric properties with simple stochastic rules. The model is validated against published experimental pool boiling data, showing excellent agreement with the boiling curve, as well as with the activation of nucleation sites, in a statistical sense. The sensitivity of the model parameters is studied to assess their influence and relevance. The model also provides information about the behavior of other near-wall relevant quantities, such as the interfacial area density and bubble detachment frequency. The computing time is around two orders of magnitude lower than the required by continuum methods to simulate pool boiling.

© 2017 Published by Elsevier Ltd.

1. Introduction

Since the 1950s, the wettability of surfaces has been identified as a key parameter in heat transfer applications [44,17]. As reviewed in Attinger et al. [3], wettability is controlled by two surface parameters, texture and chemistry. The wettability is typically quantified by the contact angle. Recently, there has been interest in surfaces with extreme values of wettability, because of their demonstrated potential to enhance and control heat transfer, as recently reviewed in Lu and Kandlikar [37] and Attinger et al. [3]: those surfaces are called superhydrophilic if a liquid drop spreads on it with a zero or nearly zero apparent contact angle, or superhydrophobic if it beads on the surface with a contact angle larger than 145° [31]. The theoretical description of surfaces with extreme values of wettability originates with Wenzel [51] and Cassie and Baxter [9]. Wenzel assumed that the liquid-solid interface follows the surface roughness, whereas according to Cassie and Baxter, air is trapped in the surface and results in partial blockage of the liquid access.

In pool boiling, for very low values of the superheat temperature, hydrophobic and superhydrophobic surfaces have been

shown to promote nucleation [17,5,50]. This enhancement has been explained by considerations on the Gibbs free energy and shown to be due to the surface chemistry and the natural presence of pits and cavities [11]. At low superheat values, below 5 K, the heat transfer coefficient was found to be higher for engineered silicon surfaces with higher values of the contact angle [5].

For high values of the superheat temperatures, transition from nucleate to film boiling occurs, a regime for which the thermodynamic efficiency is significantly decreased. The highest heat flux in the nucleate boiling regime is called CHF. Optimizing CHF can be seen as maximizing the heat transport, in the sense implied by the first principle of thermodynamics. A first attempt to model CHF was completed by Zuber [53] considering that at high heat flux single bubbles coalesce to form vapor columns. A velocity shear between the bulk liquid and these columns is induced by buoyancy, and CHF occurs from the resulting Helmholtz instability that merges columns into a vapor layer, insulating the heated solid surface from the liquid. Lienhard and Dhir [32] refined this model, assuming that the pitch between the columns equals the wavelength of Rayleigh-Taylor instabilities. The effect of wettability on CHF was modeled analytically by Kandlikar [29], who proposed that CHF occurs when the momentum flux caused by evaporation at the contact line overcomes gravity and surface tension forces, creating a vapor blanket. The results suggest that a hydrophilic surface delay the CHF occurrence. This result has been confirmed experimentally [34,43] and using a semi-analytical approach by

* Corresponding author.

E-mail addresses: christian.marcel@cab.cnea.gov.ar (C. Marcel), clausse@exa.unicen.edu.ar (A. Clause), franki@iastate.edu (C. Frankiewicz), arbetz@ksu.edu (A. Betz), attinger@iastate.edu (D. Attinger).

Li et al. [35]. In the latter, heat transfer contribution due to latent heat and transient conduction were shown to increase with superheat and contact angle. It was also shown that the natural convection cannot be neglected even if the heat flux is reaching CHF.

Some of the attempts to numerically model a pool boiling curve from first principles have been reviewed in Shoji [45] and Dhir et al. [18]. Among the numerical techniques reviewed were semi-analytical methods, and continuum methods such as volume-of-fluid and level-set methods. While these continuous numerical methods provided valuable insight for the nucleate boiling regime and the film boiling regime, the conclusions of the review were that significant effort needed to be made, in terms of modeling and computing power, to resolve the complete boiling curve, especially the transition to critical heat flux. Abarajith et al. [2] simulated bubble merger in pool boiling, with comparisons to experiments under microgravity conditions. Other continuum simulations of bubble nucleation and nucleate boiling with continuum numerical methods have been performed by Malan et al. [38] and Tryggvason et al. [47]. In those continuum models, the wetting angle can be varied over a determined – and usually relatively narrow – range of values by adapting the value of the Hamaker constant [1]. To date, the use of full three-dimensional simulations of nucleate boiling with continuum methods is limited by the enormous computing power and memory requirements [18]. Gong and Cheng [22] used the lattice Boltzmann method to simulate boiling. Their results showed that the nucleation temperature increases with the increasing heat flux for the same contact angle, and decreases with increasing contact angle for the same heat flux. Jiang et al. [27] presented a dynamic boiling model combining a continuum-based CFD model with analytical relations for the microlayer and thermal boundary layer.

While the current continuum modeling abilities are not yet able to predict a boiling curve on a surface with uniform roughness and wetting properties, a wealth of experimental data has been produced, including boiling measurements on extremely complex surfaces, with e.g. non-uniform wettability and structure. Such abilities to generate patterns or gradients of wettability are summarized in Lu and Kandlikar [37] and Attinger et al. [3]. These surfaces engineered at multiple scales (from nm to mm) have demonstrated potential for enhancing heat transfer by promoting various boiling mechanisms in the surface neighborhood. However, due to the inherent complexity and interactions of these mechanisms, it is not clear that continuum simulation methods will ever be able to capture the related physics. Thus, the heat transfer community has sought to develop alternatives to continuum models, with faster run times and improved ability to handle patterned surfaces.

The first attempts to represent the bubbly field in pool boiling by means of bubble populations are models based on the interfacial area density [23,6,7]. Those seminal models showed that it is possible to simulate pool boiling CHF as a local sudden coalescence transition. While the outcomes of this approach were further validated by experiments [8], the underlying mathematical representation still relied in macroscopic averages of local magnitudes representing void fraction, number of bubbles per unit volume, and interfacial area density. An alternative for modeling complex phenomena of statistical nature, like boiling heat transfer, is the paradigm of cellular automata [26]. Along this line, pool boiling was numerically simulated with certain degree of success by means of 2D cellular automata representing the fluid (liquid or vapor) layer adjacent to the heater wall [28], and 3D coupled lattice [24]. However, it is difficult to represent the bubble-population dynamics with this kind of rigid-grid representation. To overcome this problem, Herrero et al. [25] proposed the concept of geometric automata, where bubbles are simulated as an assem-

bly of disks that interact according to simple rules. Marcel et al. [39] applied the concept to produce a 3D model of automata for pool boiling heat transfer consisting in collections of virtual spheres. The model showed good results for simulating boiling heat transfer, bubble formation, and critical heat flux, in small heaters. In the present article the pool boiling automata framework is extended to take into account the influence of the contact angle. The new model is then validated against experimental data of heat flux and number of active sites previously measured in two specially engineered surfaces [4,5].

2. Model

Let us consider a pool boiling scenario consisting of a small heater plate placed horizontally in a container filled with stagnant refrigerant, for example water at atmospheric pressure. The model is divided in three domains: the heat conduction process in the heater material, the two-phase flow field near the heated surface, and the heat transfer mechanisms that couple the former with the latter.

2.1. Cellular-automata model of heat conduction

The heater is represented by cellular automata forming a regular square grid. A single time-varying positive real scalar variable, T_i , is assigned to each heater cell i , representing the cell temperature. The rules governing the evolution of the thermal state of the cells are based in a discrete version of the Fourier equation, that is:

$$T_i(t + \tau) = T_i(t) + Fo \left[\sum_n T_n(t) - 4T_i(t) + \frac{qL}{k_m} \right] \quad (1)$$

where the summation is performed over the cells neighboring the i -cell, t is the time, τ the time step, Fo is the Fourier number, q is the net cellular heat source defined in Section 2.3, L the cell side and k_m the heater thermal conductivity. Fo should be lower than $1/6$ in order to grant stability of the scheme.

2.2. Bubble automata

Following previous versions of the model, a population of free bubbles in the control volume attached to the heater is simulated by means of geometrical automata [25,39]. Each free bubble is codified as an automaton represented by a sphere. The state of such automaton is given by a scalar corresponding to the radius, r_b , and a vector indicating the position of the center. The following set of rules applies iteratively to the whole set of spheres:

- Displacement** (Fig. 1a): the center of each sphere moves upwards considering a terminal velocity as suggested by Wallis [49] for single bubbles. In addition, a constant distance in a random direction is added at each step to simulate turbulence. The value of such a distance is taken as half of the displacement due to buoyancy.
- Coalescence** (Fig. 1b): when two or more bubbles collide, they coalesce no matter their relative velocity, giving birth to a new bubble conserving the total volume and center of mass. This rule is in accordance with observations reported in literature (e.g., see Fig. 17 from Chen and Chung [10]).
- Breakup** (Fig. 1c): each bubble is allowed to breakup into two bubbles conserving the total volume, with a probability p per time unit given by:

$$p = \frac{r_b^2}{r_b^2 + r_c^2} \quad (2)$$

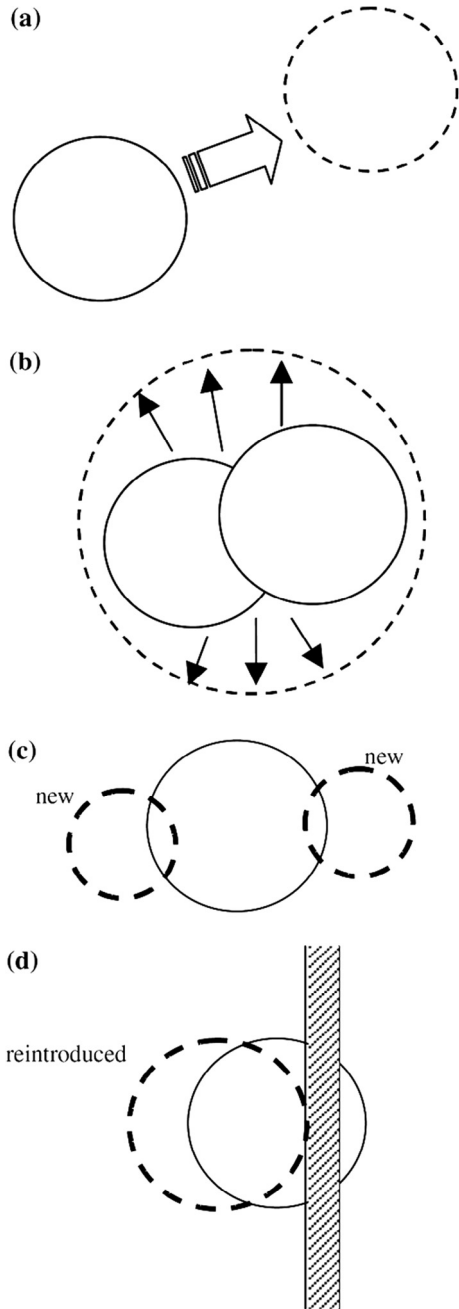


Fig. 1. Rules of the bubble automata. (a) Displacement, (b) coalescence, (c) breakup, (d) confinement.

where r_b is the bubble radius, r_c is a critical radius. In the present case, we used the value $r_c = 1.8$ -mm, calibrated for water vapor bubbles at atmospheric pressure by Marcel et al. [39].

d. Confinement (Fig. 1d): any bubble moving out of the tube environment through a lateral wall is reintroduced attached to the border.

2.3. Heat-transfer model

Although great efforts have been devoted to clarify the heat transfer mechanisms present in nucleate boiling (see e.g. [41,42,21]), still discrepancies exist regarding the modeling of such complex phenomenon. In this work a simple approach is preferred instead of more complex ones such as those presented in Moghad-

dam and Kiger [42] because these are not fully validated for boiling water.

The bubble generation is simulated with a model of heat removal accounting for four different mechanisms, which remove thermal energy from the upper layer of cellular automata of the heater and transfer it to the control volume of liquid (Fig. 4), namely:

- Natural convection, q_{nc} : continuous removal of heat by free convection to the liquid; acting over an area equal to A_{nc} .
- Microlayer evaporation, q_{me} : it is assumed that the mass evaporating into the forming bubble comes from the evaporation of the superheated microlayer located between the heater surface and the bubble [46].
- Microconvection, q_{mc} : enthalpy transport represented by the removal of the superheated liquid layer in the vicinity of the detaching bubbles, represented by an area equal to A_{mc} .
- Radiation, q_{rad} : radiation heat transferred from dry patches of the heater area to the liquid.

The total heat extracted from a given cell in contact with the liquid, q_{out} , is thus given by:

$$q_{out} = q_{nc} + q_{mc} + q_{me} + q_{rad} \quad (3)$$

The net cellular heat term, q , is the difference between the power source generated in the cell, the heat conduction process within the heater neighbor cells, and the extracted heat according to the aforementioned mechanisms.

2.3.1. Nucleation sites and the effect of the contact angle

Each cell of the heater is provided with a nucleation site at the center. The radii of the sites are randomly distributed according to a certain normal distribution. When a site is active, a bubble grows attached to the cell until a critical detachment radius, r_d , is reached, starting the growth process again with a second bubble, and so on. All detached bubbles follow the rules of the bubble geometric automata as described in Section 2.2.

Previous versions of the model did not take into account the effect of the contact angle ϕ on the site activation process. The central motivation of the present study is the inclusion and analysis of this feature using the automata model. Accordingly, a given site is active if its radius, r , satisfies [48, v. 1, p. 130]:

$$r_{\min} < r < r_{\max} \quad (4)$$

where

$$r_{\max,\min} = \frac{\delta}{2C_1} \left(1 - \frac{\theta_s}{\theta_w} \pm \sqrt{\left(1 - \frac{\theta_s}{\theta_w} \right)^2 - \frac{4\zeta C_3}{\delta\theta_w}} \right) \quad (5)$$

with:

$$\zeta = \frac{2\sigma T_{sat}}{\rho_v h_{fg}}; \quad C_1 = \frac{1 + \cos(\phi)}{\sin(\phi)}; \quad C_3 = 1 + \cos(\phi) \quad (6)$$

where

δ : is the thermal boundary layer thickness

ϕ : is the contact angle of the fluid and the heater material

θ_s : is the liquid subcooling, i.e. $T_{sat} - T_\infty$.

θ_w : is the wall superheat of the cell containing the nucleation site, i.e. $T_w - T_{sat}$

ρ_v : is the vapor density

h_{fg} : is the latent heat of the change of phase

T_{sat} : is the saturation temperature

T_∞ : is the liquid bulk temperature

σ : is the surface tension

The thermal boundary layer thickness can be estimated as $\delta = k/h$ where k is the liquid heat conduction coefficient and h is the average heat transfer coefficient assessed using the average temperature of the heater.

Natural convection heat transfer acts in the portion of the heater surface in direct contact with the liquid, see Fig. 2. For every heat transfer cell the convection heat transfer rate is given by [40,20,33]:

$$q_{nc} = \frac{A_i k}{L} Nu(T_w - T_\infty) \quad (7)$$

where A_i is the area of the cell in contact with the liquid, T_w is the wall temperature and L is the heater side characteristic length:

$$L = \frac{A_i}{P} \quad (8)$$

being A_i and P the heater area and perimeter.

The Nusselt number is calculated as:

$$\begin{aligned} Nu &= 0.54 c_{nc} Ra^{1/4} \quad \text{if } 10^4 \leq Ra_L \leq 10^7 \\ Nu &= 0.15 c_{nc} Ra^{1/3} \quad \text{if } 10^7 \leq Ra_L \leq 10^{11} \end{aligned} \quad (9)$$

where the Rayleigh number is defined as:

$$Ra = \frac{g \beta_{ca} (T_w - T_\infty) L^3}{\nu \alpha_l} \quad (10)$$

with β_{ca} being the thermal expansion coefficient of the liquid, ν is the kinematic viscosity, and α_l is the thermal diffusivity of the liquid. The coefficient c_{nc} is included to account for border effects in small heaters and uncertainties in the prediction capabilities of the correlation.

2.3.2. Microlayer evaporation

According to the Snyder model [48, v. 2, pp. 456–458] the heat extracted during the evaporation of the microlayer is given by:

$$q_{me} = \frac{4}{3} \pi (r_{\Delta t}^3 - r_o^3) \rho_v h_{fg} \quad (11)$$

where r_o is the initial radius of the bubble spherical cap, and Δt is the time period since the last bubble detachment [12–16]. The temporal growth of the radius of the attached bubble spherical cup is given by:

$$r_{\Delta t} = 2.26 Pr^{-1/2} Ja (\alpha_l \Delta t)^{1/2} \quad (12)$$

where Pr is the Prandtl number, Ja is the Jakob number. Eq. (12) is valid until the growing bubble radius reaches the detaching critical value r_d , given by the Fritz criterion [19]:

$$r_d = \frac{1}{2} 0.0148 \phi \sqrt{\frac{2\sigma}{g(\rho_l - \rho_v)}} \quad (13)$$

where g is the gravity and ρ_l and ρ_v are the liquid and vapor densities.

When a bubble spherical cap reaches the detaching radius, r_d , it departs from the hot surface, becoming a free spherical geometrical automaton (described in Section 2.2). During such a process the vapor volume is conserved. When a bubble detaches it carries with it a fraction of the superheated thermal layer. Colder liquid from the bulk of the pool quenches the heated surface and the thermal superheated layer is reformed, see Fig. 2. According to this, the heat removal by microconvection mechanism can be calculated by [30, pp. 86–91]:

$$q_{mc} = c_l \rho_l \frac{2}{3} \pi r_d (c_{mc} r_d)^2 \left(\frac{T_w + T_\infty}{2} - T_\infty \right) \quad (14)$$

where c_l is the specific heat of the liquid, and c_{mc} is the micro convection coefficient representing the liquid volume around a bubble that is conveyed with the bubble after detachment. The recommended value of c_{mc} is about twice the bubble departure radius [30, p. 403,48, p. 168]. In the present model the value of c_{mc} was calibrated around this recommended value, and the optimum results $c_{mc} = 2.25$.

The model simulates the formation of dry patches on the heater surface by allowing that detached bubbles close to the surface intersect the wall. The fraction of the cell surface covered by a bubble is considered isolated regarding all heat transfer mechanisms except radiation. Natural convection heat transfer is proportional to the fraction of the cell surface in contact with the liquid, A_i (see Fig. 3). A_i is determined by subtracting the portion of the cell covered by a free bubble to the total cell area.

2.3.3. Radiation

The heat removed by means of radiation process is accounted in the model by

$$q_{rad} = A_f \varepsilon \sigma_s b T^4 \quad (15)$$

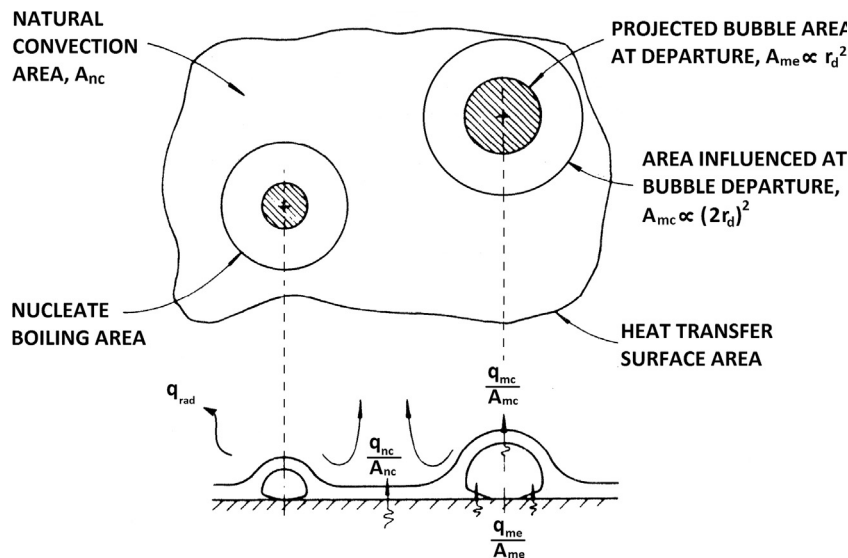


Fig. 2. Diagram of the heat transfer mechanisms modeled by the cellular automata considered in the heater.

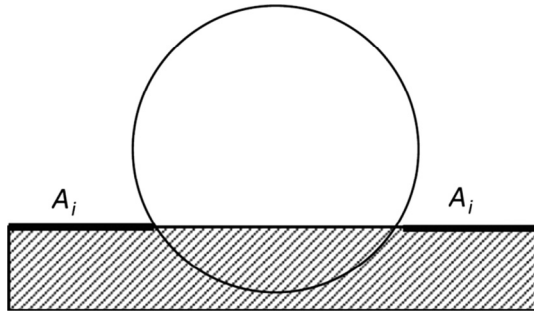


Fig. 3. Fraction of cell surface in direct contact with the liquid.

where

A_T : is the area of the cell

ε : is the emissivity of the upper surface of the heater.

σ_{sb} : is the Stefan Boltzmann constant ($\sigma_{sb} = 5.67 \cdot 10^{-8} \text{ W/m}^2 \text{ K}^4$)

3. Results

The model was applied to simulate a set of experiments performed in a pool boiling setup, as described in Betz et al. [4,5] using dedicated surfaces that produce different conditions of contact angle. The test section consists of a 1 cm side square heater made of Silicon (SiO_2), isolated from the dry side and the periphery. The heater is placed at the bottom of a liquid volume, $5 \times 5 \text{ cm}^2$ base and 4 cm height, which contains the bubble automata. The liquid is distilled and degassed saturated water at atmospheric pressure. It was verified that heat losses were rather small, estimated in 0.45 W/K. The values of the heat flux have been corrected for that loss in all reported measurements.

During the experiments, the heat transfer curve and the dependence of the number of active sites with the heater wall temperature were measured for two different contact angles, namely, 110° and 20° . The conductivity of SiO_2 is not affected by the sub micrometer layer (Teflon + Al) used to reach such a contact angle. In the experiments, the wafers had a 100 nm thickness of Teflon. The correspondent emissivity is 0.8 [52].

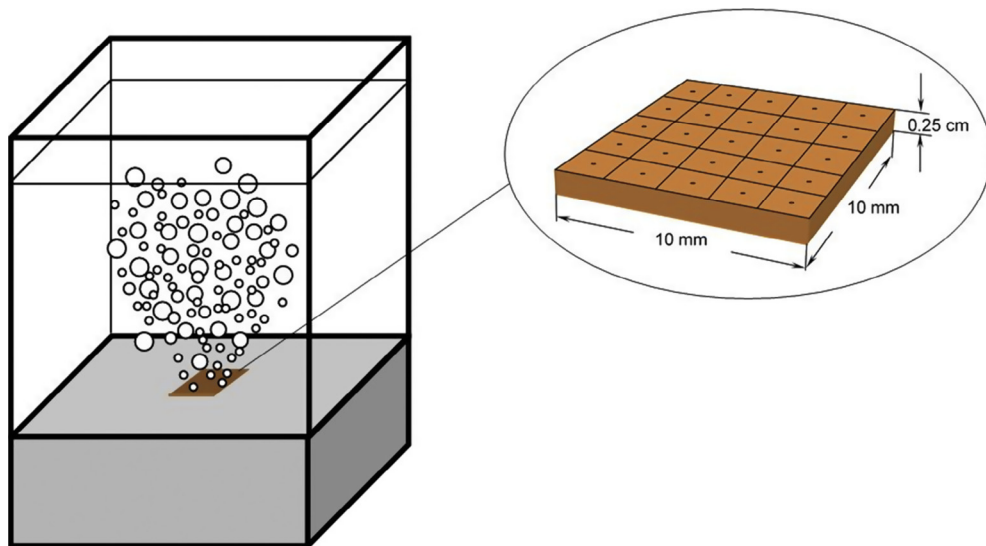


Fig. 4. Diagram of the heater and the bubble automata.

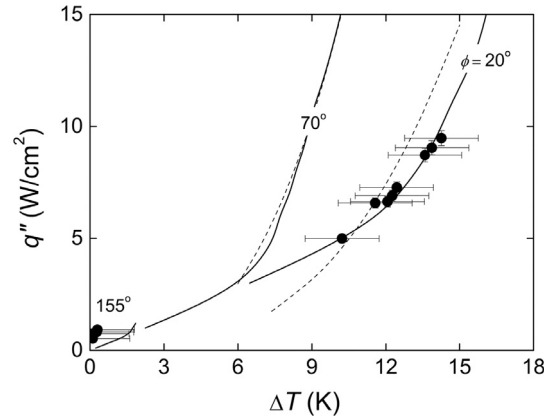


Fig. 5. Boiling curves obtained for different contact angles ϕ , experiment (symbols), present simulation with $\langle r \rangle = 5.68 \times 10^{-7} \text{ m}$ and $\sigma_r = 2.94 \times 10^{-7} \text{ m}$ (solid curves), Li et al. [36] correlation with a surface roughness of 5 nm (dashed curve).

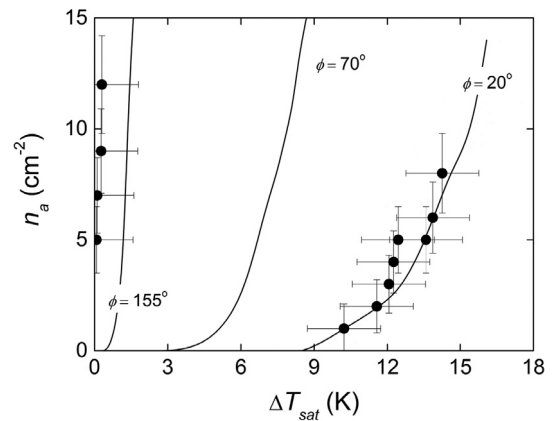


Fig. 6. Dependence of the number of active sites with the wall superheat obtained for different contact angles ϕ , experiment (symbols) and numerical simulation (curves). Reference parameters of the model: $\langle r \rangle = 5.68 \times 10^{-7} \text{ m}$, $\sigma_r = 2.94 \times 10^{-7} \text{ m}$.

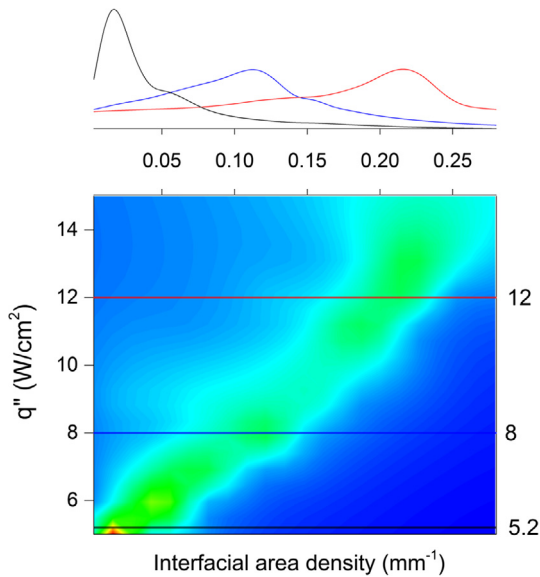


Fig. 7. Probability distribution of the interfacial area density in a control volume ($10 \times 10 \times 5 \text{ mm}^3$) directly above the heater obtained for $\phi = 20^\circ$. The color indicates the fraction of time during which the interfacial area has a certain value (horizontal axis) for a given heat flux (vertical axis). The curves of the upper graphic correspond to the cuts at constant heat flux shown in the color map at 5.2, 8 and 12 W/cm^2 . The integral below the curves is normalized to unity. (For interpretation of the references to colour in this figure legend, the reader is referred to the web version of this article.)

In the model, the heater is represented by a square grid of 6×6 cells. The power is uniformly generated over the heater cells, therefore forcing the heat flux into the water. Since the size distribution of the nucleation sites is not readily available from the experiments, and considering the different contact angles studied were obtained by fabricating surfaces with engineered wettability, the size distribution of the nucleation sites was used as a fitting parameter in the model. Specifically, a normal distribution with a

given mean cavity size and the corresponding standard deviation is assumed. The surface with 20° contact angle was taken as the reference case, for which the best estimate of the mean site radius and its standard deviation resulted $(5.68 \pm 2.94) \mu\text{m}$. The estimation corresponds to the best fit of the boiling curve at 20° contact angle. Then for any other heater characterized by a certain contact angle ϕ , each nucleation-site radius is calculated by using the following relation:

$$r_s(\phi) = a(\phi) r_{ref} - b(\phi) \quad (\text{for } \phi \geq 20^\circ) \quad (16)$$

where r_{ref} is the radius statistically calculated for the reference case. The functions a and b were the best fitting found from the experimental data at $\phi = 20^\circ$ and 155° degree.

$$\begin{aligned} a(\phi) &= (\phi - 11)/9 \\ b(\phi) &= 2.28 \times 10^{-8}(\phi - 20) \mu\text{m} \end{aligned} \quad (17)$$

It was observed that the nucleation sites become smaller and its distribution narrower when reducing the contact angle ϕ .

The other parameter that needs calibration, since it is affected by the geometry of the experimental setup, is the single-phase natural-convection factor c_{nc} , whose optimal value was found to be equal to 0.4.

Figs. 5 and 6 show the boiling curve and dependence of the number of active nucleate with the wall superheat. The simulations were performed at constant heat flux, emulating the experimental procedure. It can be seen that the model is able to reproduce very well the experimental data for contact angles 20° and 155° . An extrapolated trend for an intermediate contact angle 70° is also shown in the graphics for comparison. Note that the same values of the convective coefficients were used for all contact angles, namely, $c_{nc} = 0.4$ and $c_{mc} = 2.25$. The sensitivity of the model to the mentioned parameters is later assessed. Fig. 5 also compares a recent correlation of the pool boiling [36] valid for various surface types and contact angles ($0^\circ < \phi < 90^\circ$). It can be seen that, despite the prediction capability of the present code for contact angles different from 20° and 155° needs to be further confirmed, the agreement with Li correlation is excellent.

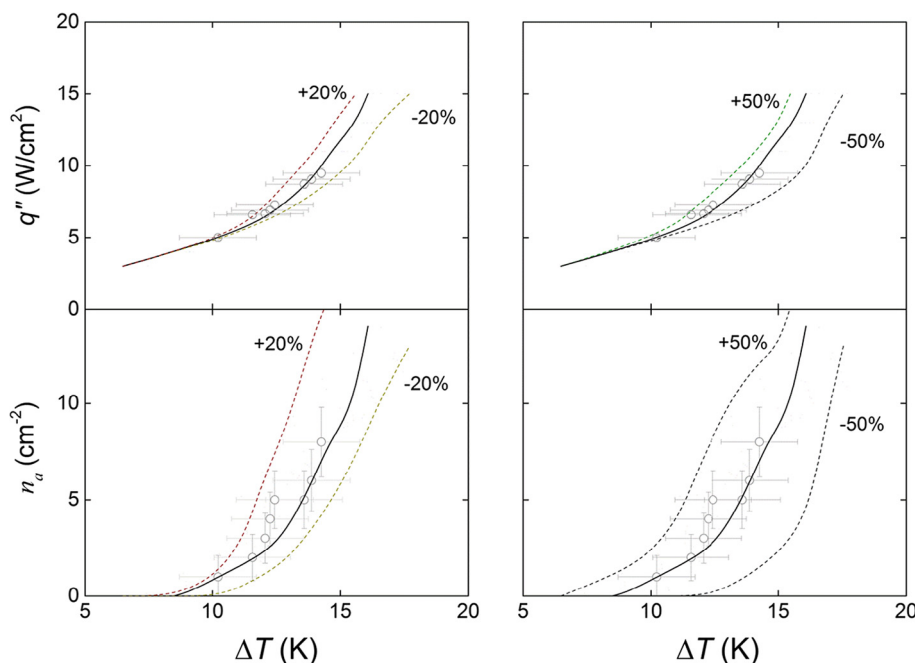


Fig. 8. Sensitivity analysis respect to variations of the radius distribution of nucleation sites: mean radius (left) and standard deviation of the radii (right). These results were obtained for $\phi = 20^\circ$.

It should be stressed that the numerical results are statistical, in the sense that the curves represents average values taken over a large number of trials. From this perspective, the present automation represents a sophisticated model that captures the complex physics of the pool boiling process. The statistical nature of the results are elucidated in Fig. 7, which shows the evolution of the probability distribution of the interfacial area density in a small control volume ($10 \times 10 \times 5 \text{ mm}^3$) directly above the heater, reported as the bubble population for each power input at a 20° contact angle. It can be seen that, as expected, the interfacial area density at low power is concentrated in a narrow range around 0.02 mm^{-1} , which corresponds to a bubble population with the size of the detaching radii. As the heat flux increases the number of bubbles increases, and so does the interfacial area. In the range between 9 and 10 W/cm^2 the distribution widens considerably, which can be explained by the coalescence of bubbles. Finally, increasing the power beyond 11 W/cm^2 , the coalescence balance in the control volume stabilizes, and the interfacial area density concentrates around 0.22 mm^{-1} .

The sensitivity of the model to several input parameters was studied for the surface with a contact angle of 20° . Fig. 8 shows the sensitivity of the results with respect to variations of the mean nucleation-site radius and its standard deviation. Changes in the sites distribution mainly affect the number of active sites dependence with ΔT . In particular, it can be observed that increasing the average site radius facilitates the activation of sites, resulting in a displacement of the boiling curve to lower temperatures. That is, for a given power the wall temperature is lower because more nucleation sites can remove heat away from the heater. When the standard deviation of the radii is reduced while keeping the same average radius, the heater wall needs to reach higher superheat to start nucleating bubbles, for there are no sites ready to activate at relatively low superheats. In turn, the standard deviation of the radii has little influence in the boiling heat transfer curve.

Fig. 9 shows the sensitivity respect to the microconvection and the single-phase natural-convection coefficients. The average number of active sites for a given wall superheat was found statistically independent of both convective coefficients. There is a slight

influence of c_{mc} in the boiling curve especially at higher fluxes. In turn, the boiling curve is very sensitive to the single-phase natural convection coefficient.

Finally, Fig. 10 shows the dependence of the average bubble departure frequency with the heat flux, calculated for the reference case of contact angle 20° . The bubble departure frequency of each site is assessed by calculating the maximum of the Fourier spectrum of the temporal evolution of the bubble radius. The graphic shows the average of all the active nucleation sites of the heater. For saturated pool boiling, a recommended empirical correlation for the bubble frequency times the departure diameter is the following [48, p. 171]:

$$f_b D_d = 1.18 \left(\frac{t_p}{t_p + t_d} \right) \left[\frac{\sigma g (\rho_l - \rho_v)}{\rho_l^2} \right]^{\frac{1}{4}} \quad (18)$$

where t_p is the average growing time of a bubble and t_d is the average time lag between consecutive bubbles. These two parameters can be calculated using the evolution of the bubble radius in each

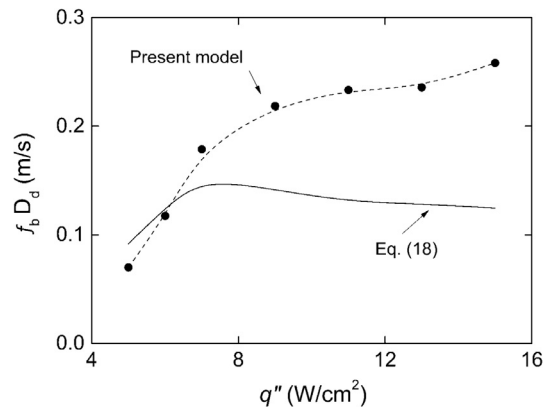


Fig. 10. Product of the bubble frequency per nucleation site times the departure size for contact angle 20° . The solid curve corresponds to the correlation given by Eq. (18).

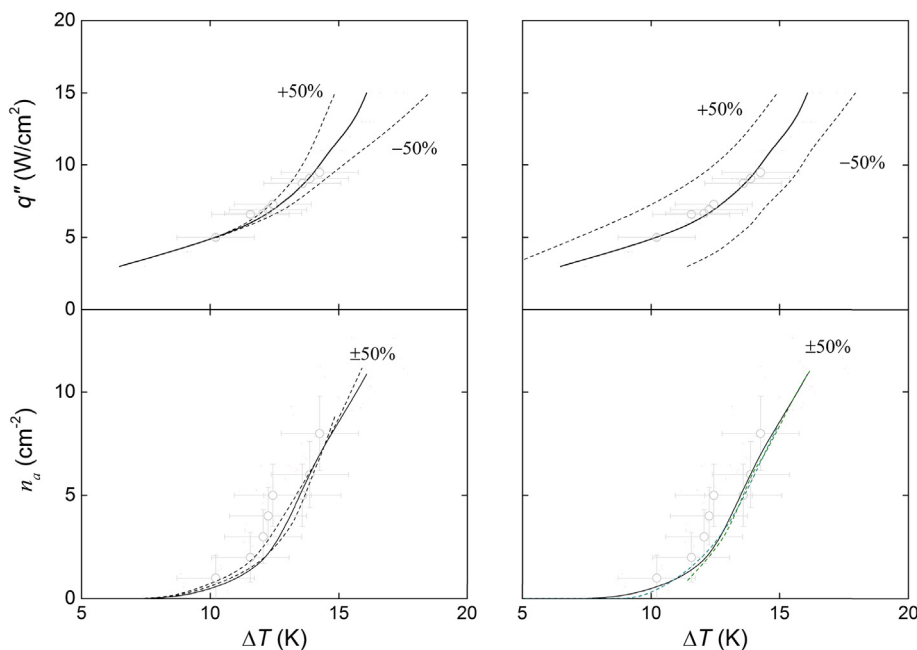


Fig. 9. Sensitivity analysis respect to variations of the micro convection coefficient c_{mc} (left) and natural convection coefficient c_{nc} (right). Reference values: $c_{mc} = 2.25$, $c_{nc} = 0.4$, $\phi = 20^\circ$.

active nucleation site given by the model. The solid curve in Fig. 10 corresponds to Eq. (18).

4. Conclusions

A model of geometric automata emulating a population of spherical bubbles that change their geometrical properties according to stochastic transition rules was developed and validated against experimental data. This type of models has showed capabilities for reproducing the heat-transfer curve in pool boiling in a statistical sense. In the present article, the influence of the contact angle was introduced, by restraining the activation of nucleation sites according to accepted mechanistic relations.

The results showed excellent agreement with experimental data of pool boiling experiments on small heaters with special surfaces with different wettability. The wettability is represented in the model by the contact angle, which influences the detachment radii. The detachment frequency results from the coupling of the whole set of magnitudes, namely, heat flux, detachment radii, radii growth rate, activation of the sites, microconvection, microlayer evaporation, natural convection, radiation and bubbles interaction.

The dependence of the heat flux and the activation of nucleation sites with the wall superheat is reproduced correctly by the model in a statistical sense. Also, the model provides information about the behavior of relevant near-wall relevant field magnitudes of the boiling phenomena, as the interfacial area density and bubble detachment frequency. Regarding the sensitivity of the model to the heater discretization, the numerical tests showed that the results are the same for finer grids. This is explained by the fact that an active nucleation site inhibits the activation of its neighbors. Hence, increasing the density of nucleation sites has null effect.

Regarding the numerical performance, using an Intel i7 processor a single time step takes about 12 microseconds of calculation. For stable time steps of 200 ns sufficient statistics could be achieved with 1-h calculation per case. Since the explicit nature of the algorithm is easily parallelizable, this time can be significantly reduced to few minutes using current GPU technology or a cluster of processors. This computing time is at least two orders of magnitude smaller than continuum simulations, which can take up to several days for the nucleation, growth and departure of a single bubble [38].

References

- [1] H. Abarajith, V. Dhir, A numerical study of the effect of contact angle on the dynamics of a single bubble during pool boiling, in: Proceedings of IMECE2002, ASME International Mechanical Engineering Congress & Exposition, New Orleans, Louisiana, 2002.
- [2] H. Abarajith, V. Dhir, G. Warriar, G. Son, Numerical simulation and experimental validation of the dynamics of multiple bubble merger during pool boiling under microgravity conditions, *Ann. New York Acad. Sci.* 1027 (2004) 235–258.
- [3] D. Attinger, C. Frankiewicz, A. Betz, T. Schutzius, R. Ganguly, A. Das, C. Kim, C. Megaridis, Surface engineering for phase change heat transfer: a review, *MRS Energy Sustainability* 1 (2014).
- [4] A. Betz, J. Xu, H. Qiu, D. Attinger, Do surfaces with mixed hydrophilic and hydrophobic areas enhance pool boiling?, *Appl Phys. Lett.* 97 (2010) 141909.
- [5] A. Betz, J. Jenkins, C. Kim, D. Attinger, Boiling heat transfer on superhydrophilic, superhydrophobic, and superbiphilic surfaces, *Int. J. Heat Mass Transf.* 57 (2013) 733–741.
- [6] P. Carrica, A. Clause, A mathematical model of local boiling nonlinear dynamics and crisis, *Lat. Am. J. Appl. Res.* 24 (1994) 77–83.
- [7] P. Carrica, A. Clause, The sudden coalescence model of boiling crisis, in: *International Conference on Nuclear Reactor Thermalhydraulics, NURETH-7* 4 2452–2460, Saratoga, New York, USA, 1995.
- [8] P. Carrica, S. Leonardi, A. Clause, Experimental study of the two-phase flow dynamics in nucleate and film pool boiling, *Int. J. Multiphase Flow* 21 (1995) 405–418.
- [9] A. Cassie, S. Baxter, Wettability of porous surfaces, *Trans. Faraday Soc.* 40 (1944) 546–551.
- [10] T. Chen, J. Chung, Coalescence of bubbles in nucleate boiling on microheaters, *Int. J. Heat Mass Transf.* 45 (2002) 2329–2341.
- [11] J. Collier, *Convective Boiling and Condensation*, McGraw-Hill, 1972.
- [12] M. Cooper, The microlayer and bubble growth in nucleate pool boiling, *Int. J. Heat Mass Transf.* 13 (1969) 915–933.
- [13] M. Cooper, J. Lloyd, The microlayer in nucleate pool boiling, *Int. J. Heat Mass Transf.* 12 (1969) 895–913.
- [14] M. Cooper, J. Lloyd, Transient local heat flux in nucleate boiling, *Proceedings of the 3rd International Heat Transfer Conference*, Chicago, vol. 3, Elsevier, Amsterdam, 1966, pp. 193–203.
- [15] M. Cooper, R. Vijuk, Bubble growth in nucleate pool boiling, *Proceedings of the 4th International Heat Transfer Conference Paris*, vol. V B2.1, Elsevier, Amsterdam, 1970.
- [16] C. Costello, C. Book, C. Nichols, A study of induced convective effects on saturated pool boiling burnout, *Chem. Eng. Prog. Symp. Ser.* 61 (1963) 271.
- [17] V. Dhir, H. Abarajith, D. Li, Bubble dynamics and heat transfer during pool and flow boiling, *Heat Transf. Eng.* 28 (2007) 608–624.
- [18] V. Dhir, G. Warriar, E. Aktinol, Numerical simulation of pool boiling: a review, *ASME J. Heat Transf.* 135 (2013) 061502.
- [19] W. Fritz, Berechnung des Maximalvolumens von Dampfblasen, *Physics* 36 (1935) 379–384.
- [20] R. Goldstein, E. Sparrow, D. Jones, Natural convection mass transfer adjacent to horizontal plates, *Int. J. Heat Mass Transf.* 16 (1973) 1025–1030.
- [21] I. Golobic, J. Petkovsek, M. Baselj, A. Papez, D. Kenning, Experimental determination of transient wall temperature distributions close to growing vapor bubbles, *Heat Mass Transf.* 45 (2009) 857–866.
- [22] S. Gong, P. Cheng, Lattice Boltzmann simulation of periodic bubble nucleation, growth and departure from a heated surface in pool boiling, *Int. J. Heat Mass Transf.* 64 (2013) 122–132.
- [23] G. Guido, P. Carrica, A. Clause, M. Qazi, A bubble number density constitutive equation, *Nucl. Eng. Des.* 152 (1994) 213–224.
- [24] A. Gupta, P. Ghoshdastidar, A three-dimensional numerical modeling of atmospheric pool boiling by the coupled map lattice method, *ASME J. Heat Transf.* 128 (2006) 1149–1158.
- [25] V. Herrero, G. Guido, A. Clause, Geometrical automata for two-phase flow simulation, *Nucl. Eng. Des.* 163 (1996) 117–124.
- [26] A. Hoekstra, J. Kroc, P. Slood, *Simulating Complex Systems by Cellular Automata*, Springer Verlag, 2010.
- [27] Y. Jiang, H. Osada, M. Inagaki, N. Horinouchi, Dynamic modeling on bubble growth, detachment and heat transfer for hybrid-scheme computations of nucleate boiling, *Int. J. Heat Mass Transf.* 56 (2013) 640–652.
- [28] Y. Jing, L. Guo, X. Zhang, A numerical simulation of pool boiling using CAS model, *Int. J. Heat Mass Transf.* 46 (2003) 4789–4797.
- [29] S. Kandlikar, A theoretical model to predict pool boiling CHF incorporating effects of contact angle and orientation, *ASME J. Heat Transf.* 123 (2001) 1071–1079.
- [30] R. Lahey, *Boiling Heat Transfer: Modern Developments and Advances*, Elsevier, Amsterdam, 1992.
- [31] K. Law, Definitions for hydrophilicity, hydrophobicity, and superhydrophobicity: getting the basics right, *J. Phys. Chem. Lett.* 5 (2014) 686–688.
- [32] J. Lienhard, V. Dhir, Hydrodynamic prediction of peak pool boiling heat fluxes from finite bodies, *ASME J. Heat Transf.* 95 (1973) 152–158.
- [33] J. Lloyd, W. Moran, Natural Convection Mass Transfer Adjacent to Horizontal Surfaces of Various Platforms, *ASME, 4-WA/HT-66*, 1974.
- [34] C. Li, Z. Wang, P. Wang, Y. Peles, N. Koratkar, G. Peterson, Nanostructured copper interfaces for enhanced boiling, *Small* 4 (2008) 1084–1088.
- [35] Y. Li, Z. Liu, G. Wang, A predictive model of nucleate pool boiling on heated hydrophilic surfaces, *Int. J. Heat Mass Transf.* 65 (2013) 789–797.
- [36] Y. Li, Y. Chen, Z. Liu, A uniform correlation for predicting pool boiling heat transfer on plane surface with surface characteristics effect, *Int. J. Heat Mass Transf.* 77 (2014) 809–817.
- [37] Y. Lu, S. Kandlikar, Nanoscale surface modification techniques for pool boiling enhancement: a critical review and future directions, *Heat Transf. Eng.* 32 (2011) 827–842.
- [38] L. Malan, R. Scardovelli, S. Zaleski, Using extrapolation techniques in VOF methodology to model expanding bubbles, *Proc. IUTAM* 15 (2015) 228–235.
- [39] C. Marcel, F. Bonetto, A. Clause, Simulation of boiling heat transfer in small heaters by a coupled cellular and geometrical automata, *Heat Mass Transf.* 47 (2011) 13–25.
- [40] W. McAdams, *Heat Transmission*, third ed., McGraw-Hill, New York, 1954 (Chapter 4).
- [41] S. Moghaddam, K. Kiger, Physical mechanisms of heat transfer during nucleate boiling of FC-72 under saturation conditions-I. Experimental investigation, *Int. J. Heat Mass Transf.* 52 (2009) 1284–1294.
- [42] S. Moghaddam, K. Kiger, Physical mechanisms of heat transfer during nucleate boiling of FC-72 under saturation conditions-II. Theoretical analysis, *Int. J. Heat Mass Transf.* 52 (2009) 1295–1303.
- [43] M. Rahman, E. Olceroglu, M. McCarthy, The role of wickability on the critical heat flux of structured superhydrophilic surfaces, *Langmuir* 30 (2014) 11225–11234.
- [44] W. Rohsenow, A Method of Correlating Heat Transfer Data for Surface Boiling of Liquids, *MIT Techn. Rep.* 5, DIC Project 6627, 1951.
- [45] M. Shoji, Studies of boiling chaos: a review, *Int. J. Heat Mass Transf.* 47 (2004) 1105–1128.

- [46] N. Snyder, Summary of Conference on Bubble Dynamics and Boiling Heat Transfer, JPL Memo 20–137, Jet Propulsion Laboratory, California Institute of Technology, 1956.
- [47] G. Tryggvason, S. Thomas, J. Lu, Direct numerical simulations of nucleate boiling, in: Proceedings of IMECE2008, October 31–November 6, 2008, Boston, Massachusetts, USA, 2009.
- [48] S. Van Stralen, R. Cole, Boiling Phenomena, McGraw-Hill, New York, 1979.
- [49] G. Wallis, One Dimensional Two-Phase Flow, McGraw-Hill, 1969, p. 248.
- [50] C. Wang, V. Dhir, Effect of surface wettability on active nucleation site density during pool boiling of water on a vertical surface, ASME J. Heat Transf. 115 (1993) 659–669.
- [51] R. Wenzel, Resistance of solid surfaces to wetting by water, Ind. Eng. Chem. 28 (1936) 988–994.
- [52] J. Zhang, J. Yu, L. Jiang, P. Liu, Analysis of the composition of infrared stealth coating and the influence factors of its emissivity, Adv. Mater. Res. 926 (2014) 56–59.
- [53] N. Zuber, Hydrodynamic Aspects of Boiling Heat Transfer PhD Thesis, UCLA, 1959.